

CompilerKV: Risk-Adaptive KV Compression via Offline Experience Compilation

Ning Yang¹ Chengzhi Wang² Yibo Liu³ Baoliang Tian⁴ Haijun Zhang⁵

Abstract

Large Language Models (LLMs) in long-context scenarios are severely constrained by the linear growth of Key-Value (KV) cache memory. Existing KV compression methods rely either on static thresholds and attention-only heuristics or on coarse memory budget allocation. Under tight memory budgets, these methods overlook two key factors: prompt-dependent variation in compression risk and functional heterogeneity across attention heads, which destabilize token selection and lead to tail failures. To address these challenges, we propose CompilerKV, a risk-adaptive and head-aware compression framework that compiles offline experience into reusable decision tables for prefill-only deployment. CompilerKV integrates two key synergistic components: (i) a Head Heterogeneity Table, learned via offline contextual bandits, which assigns head-specific reliability weights to govern functional differences across attention heads explicitly; and (ii) a Risk-Adaptive Threshold Gating mechanism that jointly models attention entropy and local perplexity, transforming prompt-level risk into deployable retention thresholds. Experiments on LongBench show CompilerKV dominates SOTA methods under a 512-token budget, recovering 97.7% of FullKV performance while achieving up to +5.2 points gain over the strongest competitor. Code and demo are available at <https://github.com/luckypiggy-orangejuice/CompilerKV>.

1. Introduction

The capability of Large Language Models (LLMs) to process extensive contexts has revolutionized applications ranging from document summarization to multi-hop reasoning (Liu et al., 2024; Bai et al., 2024). To accelerate inference, LLMs maintain a Key-Value (KV) cache that stores intermediate attention states to avoid re-computation. However, this proficiency comes at a prohibitive computational cost: the memory footprint of the KV cache grows linearly with sequence length (Behrouz et al., 2024). For a 7B model processing a 128k context, the KV cache can consume over 100GB of memory, far exceeding the capacity of standard GPUs and creating a severe bottleneck for deployment (Pope et al., 2023; Xiao et al., 2024).

To alleviate this memory pressure, KV cache compression has emerged as a critical research direction. Early approaches adopted static sparsity patterns, such as sliding windows (Child, 2019) or fixed attention sinks (Xiao et al., 2023), assuming that recent tokens and initial tokens suffice for generation. Recognizing the limitations of static retention, subsequent research evolved towards dynamic importance estimation. Methods like Heavy-Hitter Oracle (H2O) (Zhang et al., 2023) retain tokens with high accumulated attention scores. More recently, budget-aware strategies such as SnapKV (Li et al., 2024) and PyramidKV (Cai et al., 2024) have introduced structural priors to allocate memory budgets across layers, attempting to balance local precision with global context.

Despite these advances, current KV compression methods exhibit two fundamental limitations, especially in prefill-only settings under tight memory budgets. First, most approaches employ prompt-agnostic, one-size-fits-all policies that apply a global compression rate regardless of semantic complexity (Zhou et al., 2024). Under strict budgets, this leads to tail failures, where high-entropy prompts suffer severe information loss while low-entropy prompts retain redundant tokens. Second, token eviction decisions are often unstable because they rely on weakly conditioned, instantaneous attention statistics. Such signals are inherently noisy and affected by scale bias, where large magnitudes do not necessarily correspond to semantic importance. Without mechanisms to separate reliable signals from noise, small

¹Institute of Automation, Chinese Academy of Sciences, Beijing, China ²University of Electronic Science and Technology of China, Chengdu, China ³The Chinese University of Hong Kong, Shenzhen, China ⁴ByteDance, Beijing, China ⁵University of Science and Technology Beijing, Beijing, China. Correspondence to: Ning Yang <ning.yang@ia.ac.cn>.

estimation errors can shift selection boundaries and irreversibly remove critical context.

Motivated by the instability of prompt-agnostic and weakly conditioned compression strategies, we frame prefill-only KV compression as an irreversible one-shot decision under tight memory budgets. Since decisions are fixed before decoding, unstable token selection can permanently discard critical context and trigger tail failures. This perspective motivates a shift from reactive pruning to a compile-time decision paradigm, embodied by **CompilerKV**. Our contributions can be summarized as follows:

- A novel prefill-only KV cache compression framework, CompilerKV, has been proposed, which compiles offline compression experience into reusable decision tables. By jointly modeling prompt-level risk and head heterogeneity, it transforms noisy importance signals into stable decisions, injecting stabilization priors at prefill to enable robust compression without online adaptation.
- We reframe prefill-only KV compression as an irreversible one-shot decision problem under tight memory budgets and substantiate this paradigm by deriving an attention approximation error bound (Theorem 4.1), theoretically explaining how our head-aware strategy mitigates tail failures under strict memory constraints.
- Experimental results on LongBench across 16 datasets and 4 LLM backbones show that CompilerKV consistently outperforms state-of-the-art baselines under strict budgets. Under a strict 512-token budget, it recovers over **97%** of FullKV performance and surpasses the strongest competitor by up to **5.2** on complex summarization.

2. Related Work

Token Importance Estimation for Prefill-only Compression. KV compression has evolved from static sparsity patterns (Child, 2019; Roy et al., 2021) to dynamic importance estimation. To retain critical historical states, accumulation-based methods such as H2O (Zhang et al., 2023) and StreamingLLM (Xiao et al., 2023) identify heavy-hitter tokens that consistently attract high attention scores. In the specific context of prefill-only compression, SnapKV (Li et al., 2024) adapts this by utilizing an observation window at the end of the prompt to predict future relevance, performing one-shot pruning before generation begins. Recent efforts such as Value-Aware Token Pruning (VATP) (Guo et al., 2024) attempt to refine utility estimation by incorporating the absolute L_2 -norm of value vectors alongside attention probabilities. However, a direct application of these metrics often leads to tail failures, where generation

collapses due to the irreversible loss of a few key tokens. This necessitates a more robust utility metric that decouples usage frequency from information density and calibrates signal scales within each sample.

Functional Heterogeneity of Attention Heads. Beyond token-level metrics, recent studies highlight functional heterogeneity, showing that a few retrieval heads drive long-context capabilities (Fu et al., 2024; Feng et al., 2024) demonstrating that a small subset of retrieval heads dominates long-context capabilities. While approaches such as ZigZagKV (Zhong et al., 2025) attempt to exploit this by calculating head-specific importance scores during the prefill phase, they typically overlook the critical reliability gap between heads. This limitation is further supported by prior work (Voita et al., 2019), which shows that attention heads in LLMs exhibit strong functional heterogeneity and that many heads are redundant or noisy. These noisy attention heads can interfere with the recognition of key tokens, especially under high compression ratios (Du et al., 2025). Furthermore, many existing head-aware strategies (Zhang et al., 2023; Liu et al., 2023b) rely on online feedback during decoding or necessitate complex alterations to the KV cache layout, rendering them unsuitable for efficient, zero-overhead deployment in strictly prefill-only compression scenarios.

Risk-Adaptive Budgeting and Threshold Gating. Complementary to importance scoring and head heterogeneity, effective KV compression also depends on how memory budgets are allocated. Methods such as PyramidKV (Cai et al., 2024) assign larger budgets to lower layers and smaller ones to higher layers, while DynamicKV (Zhou et al., 2024) introduces task-aware budget shaping. Although these strategies improve coarse budget utilization, they largely assume similar compressibility across prompts, which limits robustness under heterogeneous inputs (Tang et al., 2025). Recent work has begun to incorporate statistical signals into caching decisions. Entropy-based approaches (Tang et al., 2024) leverage attention distributions to assess structural concentration, but often miss semantically sensitive samples with deceptively concentrated patterns. Conversely, KVPruner (Lv et al., 2025) shows that perplexity, as a measure of predictive uncertainty, provides a complementary semantic signal. We propose a Risk-Adaptive Threshold Gating mechanism that jointly models attention entropy and local perplexity, enabling robust threshold calibration for both structurally diffuse and semantically complex prompts.

3. Preliminaries

3.1. KV Caching in LLMs

LLMs are typically built upon the Transformer architecture, utilizing the Multi-Head Self-Attention (MHSA) mecha-

nism (Vaswani et al., 2017). Given an input sequence of length T , for each token at step t , the model projects its embedding into query $q_t^{(l,h)}$, key $k_t^{(l,h)}$, and value $v_t^{(l,h)}$ vectors for the l -th layer ($l \in \{1, \dots, L\}$) and h -th head ($h \in \{1, \dots, H\}$).

To accelerate autoregressive decoding, modern systems maintain a KV Cache to store historical states. For the l -th layer at step t , this cache is denoted as (K, V) , comprising all preceding keys and values: $K^{(l)} = [k_1^{(l)}, \dots, k_t^{(l)}]$, $V^{(l)} = [v_1^{(l)}, \dots, v_t^{(l)}]$. The attention mechanism relies on the attention weight $A_{j,t}^{(l,h)}$, which represents the relevance of the historical token at position j to the current query at position t :

$$A_{j,t}^{(l,h)} = \frac{\exp\left((q_t^{(l,h)})^\top k_j^{(l,h)} / \sqrt{d_{\text{head}}}\right)}{\sum_{i=1}^t \exp\left((q_t^{(l,h)})^\top k_i^{(l,h)} / \sqrt{d_{\text{head}}}\right)}, \quad (1)$$

where d_{head} is the dimension of each head and $\sum_{j=1}^t A_{j,t}^{(l,h)} = 1$. As the sequence length T increases, the memory footprint of storing $(K^{(l)}, V^{(l)})$ grows linearly with T , posing a challenge for efficient long-context inference.

3.2. Offline Reinforcement Learning

We frame the compilation of compression policies as an offline reinforcement learning (RL) problem. Since prefill compression is a one-shot decision without state transitions, we model the problem as a Contextual Bandit, i.e., a single-step Markov Decision Process (MDP).

Let $s \in \mathcal{S}$ denote a context observed at prefill time, $a \in \mathcal{A}$ as discrete compression action, and $r(s, a) \in \mathbb{R}$ as scalar reward reflecting the compression quality. Given a fixed offline dataset $\mathcal{D} = \{(s_i, a_i, r_i)\}_{i=1}^N$ collected under a behavior policy, the goal is to learn a value function $Q_\phi(s, a)$ that estimates the expected reward of each action under a given context.

Unified Reward Structure. To govern head reliability and risk thresholds, we define a unified reward function that balances compression fidelity and task-specific constraints:

$$r(s, a) = -(\mathcal{L}_{\text{comp}}(s, a) - \mathcal{L}_{\text{full}}(s)) - \lambda \cdot \Psi(s, a), \quad (2)$$

where $\Psi(s, a)$ is the task-specific penalty (e.g., budget violation), $\mathcal{L}_{\text{full}}(s)$ is the baseline loss, and $\mathcal{L}_{\text{comp}}(s, a)$ is the Negative Log-Likelihood (NLL) of the compressed model over a window Ω :

$$\mathcal{L}_{\text{comp}}(s, a) = -\frac{1}{|\Omega|} \sum_{t \in \Omega} \log P(x_t | x_{<t}, \mathbf{C}(a)), \quad (3)$$

where x_t is the ground-truth token at position t and $P(\cdot | \cdot, \mathbf{C}(a))$ represents the predicted probability distribution conditioned on the compressed KV cache $\mathbf{C}(a)$.

Optimization with Conservative Q-Learning. To mitigate the distribution shift caused by querying out-of-distribution actions, we employ Conservative Q-Learning (CQL). The universal training objective minimizes the standard Bellman error regularized by a conservative penalty:

$$\begin{aligned} \min_{\theta} \alpha & \left(\mathbb{E}_{s \sim \mathcal{D}} \left[\log \sum_{a \in \mathcal{A}} \exp(Q_\theta(s, a)) - \mathbb{E}_{a \sim \pi_\beta} [Q_\theta(s, a)] \right] \right) \\ & + \frac{1}{2} \mathbb{E}_{s, a, r \sim \mathcal{D}} [(Q_\theta(s, a) - r(s, a))^2], \end{aligned} \quad (4)$$

where π_β is the behavior policy and α controls conservatism. This approach allows robust decision table compilation for compression tasks using the same solver..

4. CompilerKV

4.1. Problem Formulation

The prefill phase processes an input prompt of length T and generates the complete KV cache $(K^{(l)}, V^{(l)})$ for each layer l . Our goal is to initialize the subsequent generation phase with a compressed, lightweight KV cache, subject to a predefined memory budget, while minimizing the degradation relative to the full KV cache. Formally, let B_l denote the token budget for layer l . We aim to select a selection set of token indices

$$\mathcal{S}^{(l)} \subset \{1, \dots, T\}, \quad \text{s.t. } |\mathcal{S}^{(l)}| \leq B_l. \quad (5)$$

The compressed KV cache $(\tilde{K}^{(l)}, \tilde{V}^{(l)})$ is then constructed by gathering the vectors corresponding to $\tilde{K}^{(l)} = K^{(l)}[\mathcal{S}^{(l)}]$ and $\tilde{V}^{(l)} = V^{(l)}[\mathcal{S}^{(l)}]$.

To find such $\mathcal{S}^{(l)}$, we propose **CompilerKV**, a framework designed for the **Prefill-only Compression** task. The overall architecture of **CompilerKV** is illustrated in Figure 1.

4.2. Stabilized Token Utility Estimation

To approximate the optimal selection set $\mathcal{S}^{(l)}$, we first establish a base utility score $u_t^{(l,h)}$ that quantifies the contribution of each historical state. Recognizing that individual attention heads can be noisy, we first aggregate signals across the entire model to form a robust baseline, and then integrate structural feature valuation.

Global Mean Attention. To mitigate the variance of single-head attention spikes, we compute the mean attention weight $\bar{A}_{j,t}$ for the token at position j by averaging the raw attention probabilities across all layers L and heads H :

$$\bar{A}_{j,t} = \frac{1}{L \cdot H} \sum_{l=1}^L \sum_{h=1}^H A_{j,t}^{(l,h)}. \quad (6)$$

Here, $\bar{A}_{j,t}$ represents the global consensus relevance of token j to the query at step t .

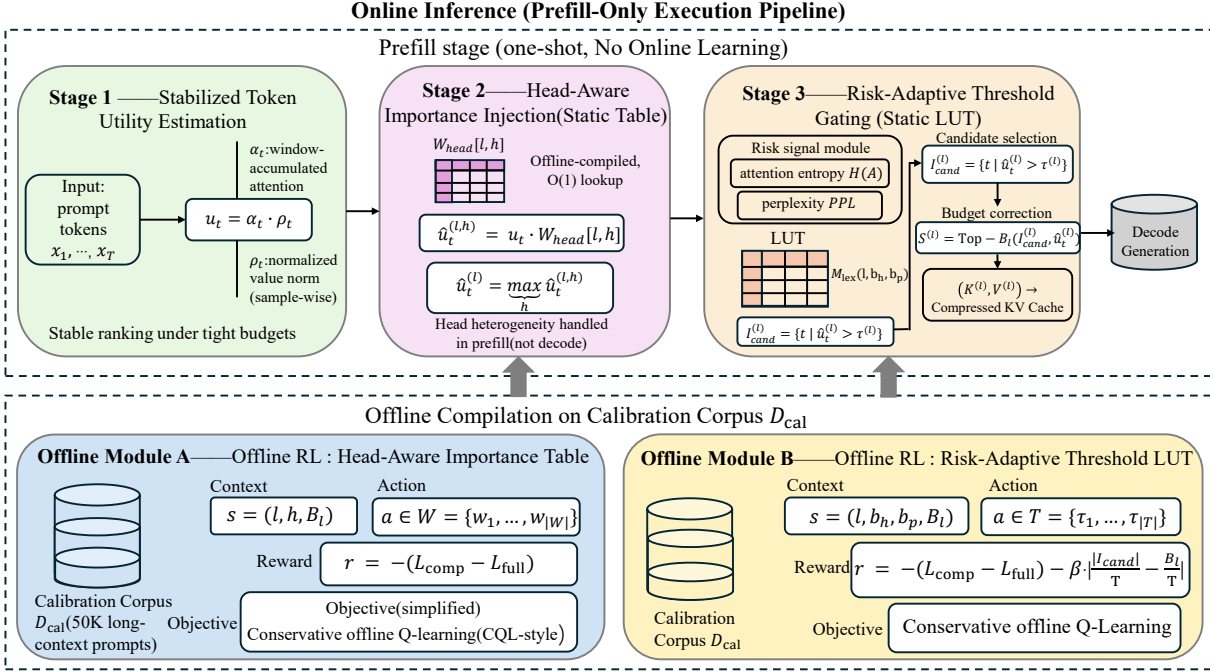


Figure 1. Overview of the CompilerKV Framework. The framework consists of three integrated stages: (1) computing a noise-resilient baseline score to filter out transient distractions; (2) modulating the ranking via a compiled Head Heterogeneity Table to strictly govern the functional differences among attention heads; and (3) querying a Risk-Gating Table to dynamically calibrate the retention threshold based on the prompt’s inherent complexity.

Window-Cumulative Attention. Instead of relying on a single step snapshot, we measure the temporal durability of a token’s influence. We define an observation window \mathcal{W} of size W at the end of the prefill phase, denoted as $\mathcal{W} = \{T-W+1, \dots, T\}$. The accumulated attention score $\alpha_t^{(l,h)}$ for a historical token is computed by aggregating attention weights across this window: $\alpha_t^{(l,h)} = \sum_{j \in \mathcal{W}} \bar{A}_{j,t}$. This aggregation smooths out transient noise, ensuring that retained tokens are those consistently attended to by the recent context rather than spurious outliers.

Relative Value Magnitude. Beyond attention probability, the information content carried by the token is encoded in its value vector $v_t^{(l,h)}$. Previous methods often utilize the absolute L_2 -norm $\|v_t^{(l,h)}\|_2$ as a proxy for importance. However, we observe that value norms fluctuate significantly across different heads and layers, leading to scale bias where layers with naturally larger norms dominate the global budget. To address this, we employ an intra-sample relative norm. We normalize $\|v_t^{(l,h)}\|_2$ by the sequence average to obtain a scale-invariant factor $\rho_t^{(l,h)}$:

$$\rho_t^{(l,h)} = \frac{\|v_t^{(l,h)}\|_2}{\frac{1}{T} \sum_{k=1}^T \|v_k^{(l,h)}\|_2}. \quad (7)$$

Unified Base Utility. The final stabilized utility score $u_t^{(l,h)}$ for the t -th token in the h -th head of layer l is derived as the

product of its cumulative relevance and relative density:

$$u_t^{(l,h)} = \alpha_t^{(l,h)} \cdot \rho_t^{(l,h)}. \quad (8)$$

This metric $u_t^{(l,h)}$ serves as the foundational signal for our framework, filtering out tokens that are either semantically irrelevant (low α) or informationally sparse (low ρ).

4.3. Head-Aware Importance Injection via Offline Table Compilation

While base utility $u_t^{(l,h)}$ captures token significance, treating heads equally ignores functional heterogeneity (e.g., retrieval vs. noisy heads). To address this, we propose a “compile-then-execute” paradigm: head reliability priors are compiled offline on a calibration corpus and deployed as a frozen lookup table to rigorously govern head contributions.

Offline Learning Framework. We instantiate the general offline RL framework (Section 3.2) to compile the **Head Heterogeneity Table** (\mathbf{W}_{head}). The MDP tuple $\langle \mathcal{S}, \mathcal{A}, r \rangle$ is defined as follows:

- **State Space (\mathcal{S}):** To learn a position-specific prior, the state encapsulates the structural coordinates and layer budget. For the h -th head in the l -th layer, the state is $s_{l,h} = (l, h, B_l)$.

- **Action Space (\mathcal{A}):** The action represents the reliability weight derived from a discretized scalar set \mathcal{W} . The selected action $a_{l,h} \in \mathcal{W}$ acts as a multiplicative modulator for the utility scores.
- **Reward (r):** We adopt the unified reward function (Eq. 2) with $\lambda = 0$, as head weighting aims purely for NLL recovery without directly triggering budget violations. We calculate the *marginal contribution* of each head by applying action $a_{l,h}$ while holding others constant.

Table Compilation. We optimize the policy using the unified CQL objective (Eq. 4) on the calibration dataset. Upon convergence, the probabilistic policy is “compiled” into a deterministic lookup table \mathbf{W}_{head} by maximizing the learned Q-value:

$$\mathbf{W}_{\text{head}}[l, h] = \underset{w \in \mathcal{W}}{\text{argmax}} Q_{\theta}(s_{l,h}, w). \quad (9)$$

This artifact captures the global importance of each attention head. Once compiled, this table is fixed and directly applied during prefill, injecting head-specific reliability priors without any online learning or runtime adaptation.

Inference: Weighted Max-Pooling. During the online prefill phase, we implement a **weighted max-pooling** strategy to grant reliable heads veto power. The final layer-wise importance score $\hat{u}_t^{(l)}$ is calculated as:

$$\hat{u}_t^{(l)} = \max_{h \in \{1, \dots, H\}} \left(u_t^{(l,h)} \cdot \mathbf{W}_{\text{head}}[l, h] \right). \quad (10)$$

This mechanism ensures that if a critical retrieval head (high weight) strongly attends to a token, that token is protected from eviction regardless of the consensus from noisy heads.

4.4. Risk-Adaptive Threshold Gating

While $\hat{u}_t^{(l)}$ incorporates head reliability, fixed Top- k strategies fail by assuming uniform compressibility. High-density samples require conservative retention to prevent tail failures, whereas low-density ones permit aggressive pruning. To address this, we introduce Risk-Adaptive Gating, which dynamically calibrates the retention threshold based on instance-specific difficulty.

Joint Risk Modeling. We quantify compression difficulty using two metrics within the observation window Ω : **Attention Entropy** $\mathcal{R}_{\text{struct}}$, which serves as the **Structural Risk** to measure the dispersion of attention patterns, and **Local Perplexity** \mathcal{R}_{sem} , which represents the **Semantic Risk** indicating predictive uncertainty.

1. **Structural Risk ($\mathcal{R}_{\text{struct}}$):** A high entropy implies that the model lacks a clear focus point (e.g., dense retrieval), making pruning riskier. Unlike previous methods that calculate step-wise entropy, we first compute

the *Global Mean Attention* \bar{A}'_t by averaging attention weights across all layers L , heads H , and window positions Ω :

$$\bar{A}'_t = \frac{1}{|\Omega| L H} \sum_{j \in \Omega} \sum_{l=1}^L \sum_{h=1}^H A_{j,t}^{(l,h)}. \quad (11)$$

The structural risk is then defined as the Shannon entropy of this aggregated distribution:

$$\mathcal{R}_{\text{struct}} = - \sum_{t=1}^T \bar{A}'_t \log \bar{A}'_t. \quad (12)$$

2. **Semantic Risk (\mathcal{R}_{sem}):** We assess predictive uncertainty using local perplexity. A spike in perplexity indicates complex semantic dependencies where historical context is critical. We calculate the exponentiated average negative log-likelihood over the window:

$$\mathcal{R}_{\text{sem}} = \exp \left(-\frac{1}{|\Omega|} \sum_{j \in \Omega} \log P(x_j | x_{<j}) \right). \quad (13)$$

Compiling the Risk Table. Instead of tuning thresholds manually, we compile a **Risk Threshold Table** (\mathbf{T}_{gate}) by instantiating the unified offline RL framework (Section 3.2). The specific MDP components are defined as:

- **State Space (\mathcal{S}):** The state captures the layer index and the discretized risk coordinates. We map the continuous risks ($\mathcal{R}_{\text{struct}}, \mathcal{R}_{\text{sem}}$) into discrete bins ($b_{\text{ent}}, b_{\text{ppl}}$). Thus, the state is defined as $s_l = (l, b_{\text{ent}}, b_{\text{ppl}}, B_l)$.
- **Action Space (\mathcal{A}):** The action corresponds to selecting a scalar retention threshold $\tau \in [0.8, 1.0]$. A lower τ retains more tokens (conservative), while a higher τ implies aggressive pruning.
- **Reward with Budget Constraint (r):** Unlike head weighting, threshold selection directly impacts memory usage. We utilize the unified reward function (Eq. 2) with a non-zero penalty weight ($\lambda > 0$). Let $\lambda = \frac{\beta}{T}$, where β is a hyperparameter. The constraint term is defined as the deviation from the target budget:

$$\Psi(s, a) = |\mathcal{I}_{\text{cand}}(a)| - B_l, \quad (14)$$

where $\mathcal{I}_{\text{cand}}(a)$ is the set of tokens retained by threshold a . This encourages the policy to find the strictness threshold that maximizes fidelity without violently violating the layer-wise budget B_l .

Final Selection: Gating with Budget Correction. The final selection set $\mathcal{S}^{(l)}$ is determined by a Threshold Gating and Top- B_l Correction strategy. First, we generate a candidate set based on the adaptive threshold:

$$\mathcal{I}_{\text{cand}}^{(l)} = \{t \mid \hat{u}_t^{(l)} \geq \tau^{(l)}\}. \quad (15)$$

To strictly enforce the hardware storage budget B_l , we apply a correction step:

$$\mathcal{S}^{(l)} = \begin{cases} \mathcal{I}_{\text{cand}}^{(l)}, & \text{if } |\mathcal{I}_{\text{cand}}^{(l)}| \leq B_l, \\ \text{Top-}B_l(\mathcal{I}_{\text{cand}}^{(l)}, \hat{u}_t^{(l)}), & \text{if } |\mathcal{I}_{\text{cand}}^{(l)}| > B_l, \end{cases} \quad (16)$$

where $\text{Top-}B_l(\mathcal{I}, u)$ denotes the subset of B_l indices from \mathcal{I} corresponding to the largest values in the score u . The first condition permits elastic retention for low-risk prompts where the adaptive threshold naturally filters out enough redundancy ($|\mathcal{I}_{\text{cand}}^{(l)}| \leq B_l$). The second condition acts as a hard clamp, prioritizing the highest-utility tokens to maximize information density when the risk-aware policy admits an excess of candidates.

KV Cache Construction. The prefill phase processes an input prompt of length T and generates the complete KV cache $(K^{(l)}, V^{(l)})$ for each layer l . Upon determining the optimal indices $\mathcal{S}^{(l)}$, the final compressed KV cache $(\tilde{K}^{(l)}, \tilde{V}^{(l)})$ is constructed by gathering the vectors corresponding to the selected indices:

$$\tilde{K}^{(l)} = K^{(l)}[\mathcal{S}^{(l)}], \quad \tilde{V}^{(l)} = V^{(l)}[\mathcal{S}^{(l)}], \quad (17)$$

where $K^{(l)}[\mathcal{S}^{(l)}]$ signifies the projection of the full Key cache onto the selected index set, effectively retaining only the feature vectors required for the compressed representation. This selection and construction process is performed *once* at the end of the prefill phase (step T). During the subsequent autoregressive decoding, the retained cache $(\tilde{K}^{(l)}, \tilde{V}^{(l)})$ remains static, prohibiting any further updates or evictions. This “compile-then-execute” paradigm ensures that the overhead of our complex selection logic is amortized to zero during generation.

4.5. Theoretical Analysis

To provide insight into the stability of CompilerKV under extreme compression, we derive a stability-oriented bound on the approximation error of the attention output.

Theorem 4.1 (Stability-Oriented Attention Approximation Bound). *Consider a transformer layer l with input sequence length T and budget B_l . Let $A^{(l,h)}$ and $\tilde{A}^{(l,h)}$ denote the full and compressed attention matrices, respectively. Under CompilerKV’s selection policy determined by the stabilized utility $\hat{u}_t^{(l)}$ and the head reliability table W_{head} , with probability at least $1 - \delta$, the layer-wise aggregated approximation error satisfies:*

$$\begin{aligned} & \frac{1}{H} \sum_{h=1}^H \left\| A^{(l,h)} - \tilde{A}^{(l,h)} \right\|_F \\ & \leq \sqrt{T} \cdot \epsilon_{\text{tail}}^{(l)} + \mathcal{O} \left(\sqrt{\frac{(T - B_l) \log(1/\delta)}{T \cdot (W_{\min}^{(l)})^2}} \right), \end{aligned} \quad (18)$$

where $\epsilon_{\text{tail}}^{(l)}$ denotes the average attention mass of discarded tokens, and $W_{\min}^{(l)}$ is the minimum reliability weight assigned to any head in layer l .

The bound shows that worst-case approximation error is dominated by discarded tail mass and is inversely controlled by head reliability weighting, explaining how stabilized, head-aware selection reduces sensitivity to noisy importance signals under irreversible prefill-only compression. The proof of Theorem 4.1 is shown in Appendix A.

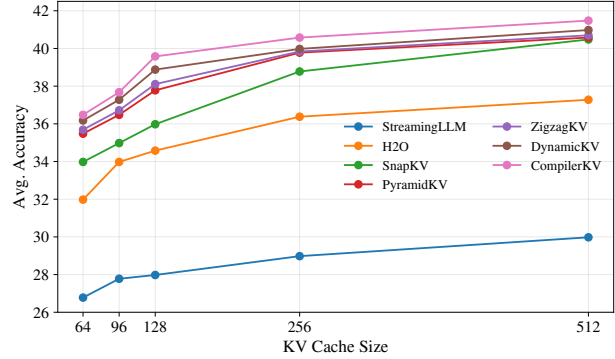


Figure 2. Performance vs. KV Cache Size. Comparison of average accuracy on LongBench across different budget constraints. Our method (CompilerKV) degrades most gracefully, maintaining usability even at extreme compression ratios where baselines fail.

5. Experiments

5.1. Experimental Setup

Datasets and Metrics. We evaluate our method on LongBench (Bai et al., 2024), a comprehensive benchmark for long-context understanding. We cover a diverse set of 16 tasks across categories including Single-Doc QA (e.g., NarrativeQA (Kočiský et al., 2018), Qasper (Dasigi et al., 2021)), Multi-Doc QA (e.g., HotpotQA (Yang et al., 2018)), Summarization (e.g., GovReport (Huang et al., 2021), Multi-News (Fabbri et al., 2019)), Few-shot Learning (e.g., TREC (Li & Roth, 2002), SAMSum (Gliwa et al., 2019)), and Synthetic & Code tasks including Passage Retrieval (PRe), Passage Count (Pcount), LCC (Guo et al., 2023), and RepoBench-P (RB-P) (Liu et al., 2023a). Following standard protocols, we report the specific metric for each dataset and the macro-average score.

Baselines. We benchmark against FullKV (theoretical upper bound) and six SOTA methods representing diverse paradigms: H2O (Zhang et al., 2023) and StreamingLLM (Xiao et al., 2023) as eviction-based baselines; SnapKV (Li et al., 2024) and ZigZagKV (Zhong et al., 2025) for prefill-optimized selection; and PyramidKV (Cai et al., 2024) alongside DynamicKV (Zhou et al., 2024) for budget allocation strategies. This selection comprehensively covers

Table 1. Main Results on LongBench (Budget = 512 Tokens). Comparisons with state-of-the-art compression methods across four LLMs. The best result among compression methods is **bolded**, and the second best is underlined.

Model	Method	Single-Doc QA				Multi-Doc QA				Summarization			Few-Shot Learning			Synthetic & Code				Avg.												
		NarrativeQA		Qasper		MF-en		HotpotQA		2WikiQA		MuSiQue		GovReport		QMSum		MultiNews		TREC		TriviaQA		SAMSum		Lcc		RIP-P		Poumt		
		FullKV	22.47	27.58	39.98	40.96	33.52	26.61	33.01	25.18	26.28	72.5	86.76	39.84	55.86	57.90	2.92	100	43.21													
InternLM-2.5 7B-Chat-1M	FullKV	22.47	27.58	39.98	40.96	33.52	26.61	33.01	25.18	26.28	72.5	86.76	39.84	55.86	57.90	2.92	100	43.21														
	StreamingKV	17.58	15.86	26.55	26.68	16.69	11.01	25.96	21.33	25.57	65.0	67.16	21.71	43.58	42.76	0.95	87.56	32.25														
	H2O	15.33	19.84	32.67	27.96	19.94	21.18	16.91	23.00	21.46	42.0	<u>84.38</u>	34.76	48.46	50.00	1.23	96.50	34.73														
	SnapKV	16.86	23.28	36.24	32.14	19.89	23.21	17.81	23.18	22.44	71.0	84.05	34.34	50.32	53.34	1.00	96.50	37.85														
	PyramidKV	17.62	21.08	37.52	32.21	21.31	22.03	19.37	24.06	22.22	73.0	83.94	34.61	50.45	49.72	1.05	95.50	37.86														
	ZigZagKV	17.28	22.07	36.94	32.18	20.67	22.56	18.67	23.66	22.32	72.0	83.99	34.49	50.39	51.35	1.03	95.95	37.93														
	DynamicKV	17.77	23.87	37.74	<u>32.98</u>	21.13	23.21	19.13	23.49	22.48	75.0	84.89	36.70	<u>50.70</u>	51.08	0.91	95.50	38.54														
LLaMA-3 8B-Instruct	Ours	18.47	24.22	38.37	33.49	<u>21.25</u>	<u>23.05</u>	<u>24.41</u>	<u>24.05</u>	<u>23.68</u>	75.0	84.31	<u>36.11</u>	51.16	52.88	1.00	95.50	39.18														
	FullKV	25.16	31.81	39.59	43.09	36.15	21.77	28.62	23.34	26.33	75.0	90.50	42.36	59.04	53.93	5.20	69.25	41.95														
	StreamingKV	19.03	12.78	28.67	37.83	29.97	16.55	20.30	20.94	24.56	61.0	75.43	30.82	51.93	49.98	5.86	69.50	34.70														
	H2O	22.84	16.80	32.36	41.50	34.07	19.33	22.28	22.88	23.69	41.0	90.46	40.22	57.52	55.43	5.54	69.50	37.21														
	SnapKV	24.62	22.78	37.88	42.96	34.82	20.25	22.63	22.54	23.93	70.0	90.39	40.30	60.27	55.85	5.74	69.50	40.28														
	PyramidKV	24.48	23.51	36.24	42.33	31.95	20.73	<u>23.37</u>	23.01	24.37	72.5	<u>90.43</u>	40.54	59.27	54.87	5.88	69.50	40.19														
	ZigZagKV	24.54	23.18	36.98	42.61	33.24	20.51	23.04	22.80	24.17	71.4	90.41	40.43	59.72	55.31	5.81	69.50	40.66														
Qwen2 7B-Instruct	DynamicKV	24.80	24.62	36.69	44.13	33.25	<u>20.82</u>	23.00	22.54	24.12	72.5	90.39	40.76	61.21	<u>56.91</u>	5.78	69.50	40.69														
	Ours	24.97	25.11	37.01	<u>43.04</u>	35.69	20.86	<u>23.66</u>	<u>22.93</u>	<u>25.40</u>	<u>72.5</u>	90.21	<u>40.67</u>	61.47	57.00	5.64	69.50	40.98														
	FullKV	25.14	42.35	45.04	14.80	14.13	9.23	36.35	23.79	26.51	76.5	89.16	45.23	60.30	60.78	6.50	75.50	40.71														
	StreamingKV	20.47	26.97	32.64	14.31	14.39	6.82	25.70	19.31	24.88	66.0	76.56	32.11	46.58	44.20	8.00	15.50	29.65														
	H2O	22.88	34.28	41.50	13.30	14.60	8.31	23.69	22.07	22.72	39.5	88.75	43.91	58.83	57.83	8.00	72.00	35.76														
	SnapKV	23.86	38.50	44.68	15.60	14.62	9.13	24.56	22.39	23.18	70.0	89.31	43.32	58.68	60.74	5.00	72.00	38.47														
	PyramidKV	24.47	37.60	43.51	14.48	12.83	8.99	23.59	22.30	22.41	74.0	89.21	43.40	57.67	56.14	6.50	74.00	38.19														
Mistral-7B Instruct-v0.2	ZigZagKV	24.19	38.01	44.04	14.98	13.64	9.05	24.03	22.34	22.76	72.5	89.26	43.36	58.12	58.21	5.80	73.00	38.80														
	DynamicKV	24.66	40.44	45.30	15.42	13.89	8.46	25.51	22.77	22.92	74.0	89.27	43.18	60.38	59.32	7.00	74.00	39.16														
	Ours	25.05	41.00	44.99	14.75	14.04	8.50	25.96	22.70	<u>24.16</u>	75.5	89.09	43.38	60.76	60.10	8.00	74.00	39.50														
	FullKV	26.63	32.99	49.34	42.77	27.35	18.77	32.87	24.24	27.10	71.0	86.23	42.96	56.93	54.49	2.75	86.98	42.71														
	StreamingKV	19.05	17.21	36.82	30.64	21.84	10.56	24.47	19.84	25.48	62.0	72.82	29.49	46.15	42.55	2.71	19.25	30.06														
	H2O	22.23	25.75	44.09	32.76	22.88	14.96	23.53	22.96	24.53	41.5	85.53	41.54	55.11	50.81	3.39	86.20	37.36														
	SnapKV	24.96	27.97	49.04	39.93	25.18	17.64	24.14	23.69	24.41	67.5	86.09	41.11	56.73	<u>53.11</u>	2.86	86.98	40.71														
Qwen2-7B Instruct	PyramidKV	23.55	28.79	48.71	41.00	25.64	16.35	<u>24.79</u>	23.52	24.49	69.5	86.20	42.58	55.45	<u>51.67</u>	3.53	81.81	40.47														
	ZigZagKV	24.18	28.42	48.86	40.52	25.43	16.93	24.49	23.59	24.45	68.5	86.15	41.91	56.03	52.32	3.22	84.14	40.83														
	DynamicKV	25.63	<u>29.11</u>	48.41	39.80	26.62	16.72	24.73	23.42	24.83	70.5	86.74	43.01	55.40	52.45	3.20	83.57	<u>40.88</u>														
	Ours	26.06	29.51	49.29	41.46	27.06	18.15	25.16	24.19	25.13	70.5	86.18	42.91	55.13	51.37	3.29	84.02	41.21														

the spectrum from accumulation-based to head-aware and risk-adaptive compression.

Implementation Details. We conduct experiments on four popular LLMs: LLaMA-3-8B-Instruct, Qwen2-7B-Instruct, Mistral-7B-Instruct-v0.2, and InternLM-2.5-7B-Chat. Unless otherwise stated, we set the KV cache budget to 512 tokens per layer for the compressed history. For our method, we *compile* both the Head Reliability Table and the Risk-Adaptive Threshold Gating on a held-out calibration corpus of approximately 50K long-context prompts, following Appendix B. This calibration corpus is strictly disjoint from all LongBench evaluation instances to avoid leakage.

5.2. Main Results: Performance on LongBench

Table 1 presents the comparative results across all models. Our method consistently outperforms all baselines and achieves performance closest to the FullKV upper bound.

Superiority over State-of-the-Arts. Under the strict 512-token budget, our method achieves the highest average scores across all four models. On LLaMA-3-8B, we achieve an average score of 40.98, surpassing the strongest baseline (DynamicKV: 40.69) and recovering 97.7% of the FullKV performance (41.95). On Qwen2-7B, while StreamingLLM and H2O suffer significant degradation (col-

lapsing to < 36.0 avg), our method maintains a robust score of 39.50, significantly outperforming ZigZagKV (38.33) which suffers from head-selection noise.

Comparison with Dynamic Budgeting. Our results show that simply moving budget to lower layers is insufficient for complex reasoning tasks (e.g., Qasper). By contrast, our method, which jointly models entropy and perplexity, successfully identifies and protects high-complexity segments, yielding a +1.17 improvement on Qasper (InternLM-2.5) compared to PyramidKV.

5.3. Analysis of Compression Robustness

To understand the behavior of our method under varying constraints, we evaluate the performance retention rate across different KV cache sizes (ranging from 64 to 1024 tokens).

Figure 2 illustrates the performance trajectory across varying budget constraints. While eviction-based baselines exhibit precipitous performance drops as the budget decreases below 256 tokens, our approach maintains a significantly flatter degradation curve.

Needle-in-a-Haystack Retrieval Heatmaps. To assess the fidelity of our compressed representations, we visualize the “Needle-in-a-Haystack” retrieval heatmaps in Figure 3. While baselines like StreamingLLM and SnapKV suf-

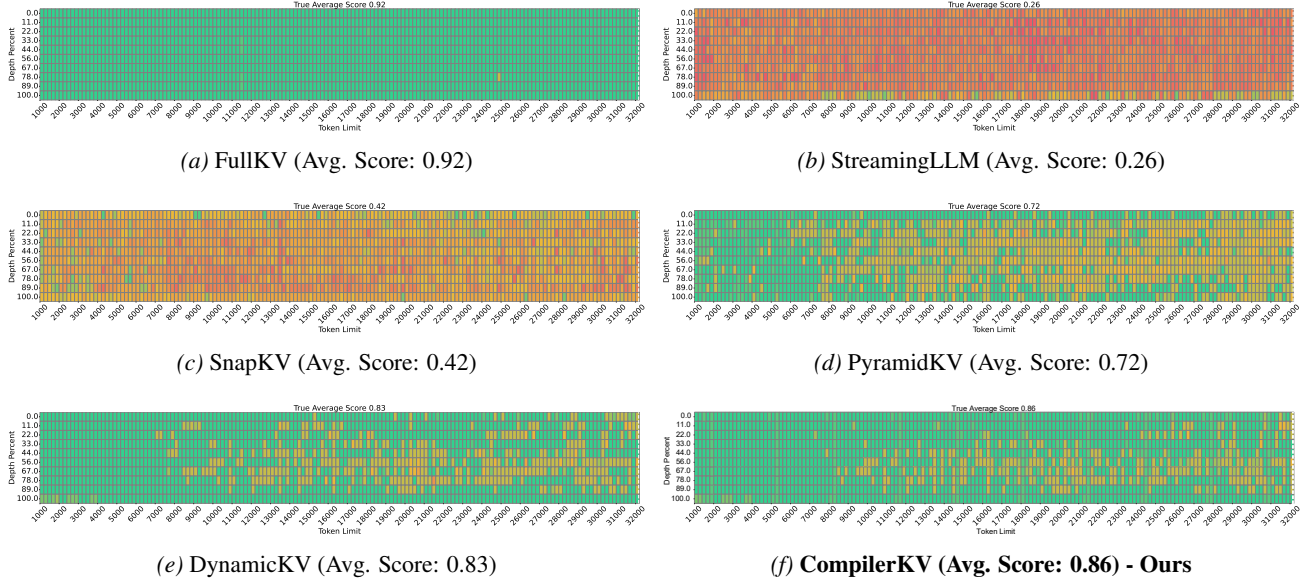


Figure 3. Needle-in-a-Haystack Pressure Test on Mistral-7B. Visual comparison of retrieval accuracy (Green=100%, Red=0%) across varying context lengths (x-axis) and needle depths (y-axis). **FullKV** (a) sets the upper bound. While baselines like **StreamingLLM** (b) and **SnapKV** (c) struggle with long-range dependencies, and **DynamicKV** (e) shows fragmentation at extreme lengths, our method **CompilerKV** (f) maintains a robust retrieval pattern comparable to the oracle.

fer severe information loss (0.26–0.42) and even strong contenders like DynamicKV exhibit fragmentation in deep contexts, CompilerKV achieves a superior score of 0.86. By adaptively preserving high-risk tokens, our method reconstructs a retrieval pattern that closely mirrors the oracle FullKV (0.92), effectively bridging the gap where other compression methods fail.

Additional Experiments. Beyond predictive accuracy, we provide the detailed profiling on end-to-end latency and peak memory usage across various context lengths in Table A1 in Appendix B.2, demonstrating up to a 60% reduction in total latency for long-sequence generation. The effectiveness of these components is further substantiated by the policy visualizations in Figure A2 and A3 in Appendix B.2, which confirm that the learned tables successfully identify retrieval heads and structurally sensitive layers.

5.4. Ablation Study

We conducted ablation experiments on Head Reliability Governance and Risk-Adaptive Gating to verify the contributions of these two core components. As shown in Table 2, Risk-Adaptive Gating proves most critical; replacing it with static thresholds causes the largest drop (~3.0 points). Stabilized Utility is also vital, as reverting to raw attention degrades performance by ~1.9 points, confirming its role in mitigating scale bias. Finally, Head Reliability contributes a consistent gain (~1.0 point) by filtering noisy heads to prioritize reliable signals.

Table 2. Component-wise Ablation Study. Impact of removing specific modules under a 512-token budget. Risk-Adaptive Thresholding (τ) is the most critical factor.

Ablation Setting	Mistral	LLaMA-3	Qwen2	InternLM
CompilerKV (Full)	41.21	40.98	39.50	39.18
w/o Head Reliability	40.26	40.13	38.60	38.38
w/o Risk-Adaptive τ	38.16	38.13	36.30	36.23
w/o Stabilized Utility	39.36	39.28	37.55	37.43

6. Conclusion

We introduced CompilerKV, a framework that fundamentally rethinks KV cache compression by treating it as a risk-adaptive compilation process rather than a static pruning task. By injecting offline-learned head reliability priors and dynamically calibrating retention thresholds based on prompt complexity, our approach successfully overcomes the inherent instability of the one-size-fits-all compression policy and scale-biased attention statistics. Empirical results across diverse architectures confirm that CompilerKV achieves near-lossless performance even under extreme memory constraints, effectively decoupling inference cost from context length. This paradigm paves the way for deploying robust long-context capabilities on memory-constrained edge devices without the performance trade-offs typical of heuristic approaches. Future work will explore extending this compilation strategy to streaming generation and investigating the transferability of reliability tables across different model families.

References

Bai, Y., Lv, X., Zhang, J., Lyu, H., Tang, J., Huang, Z., Du, Z., Liu, X., Zeng, A., Hou, L., et al. Longbench: A bilingual, multitask benchmark for long context understanding. In *Proceedings of the 62nd annual meeting of the association for computational linguistics (volume 1: Long papers)*, pp. 3119–3137, 2024.

Behrouz, A., Zhong, P., and Mirrokni, V. Titans: Learning to memorize at test time. *arXiv preprint arXiv:2501.00663*, 2024.

Cai, Z., Zhang, Y., Gao, B., Liu, Y., Li, Y., Liu, T., Lu, K., Xiong, W., Dong, Y., Hu, J., et al. Pyramidkv: Dynamic kv cache compression based on pyramidal information funneling. *arXiv preprint arXiv:2406.02069*, 2024.

Child, R. Generating long sequences with sparse transformers. *arXiv preprint arXiv:1904.10509*, 2019.

Dasigi, P., Lo, K., Beltagy, I., Cohan, A., Smith, N. A., and Gardner, M. A dataset of information-seeking questions and answers anchored in research papers. *arXiv preprint arXiv:2105.03011*, 2021.

Du, W., Jiang, L., Tao, K., Liu, X., and Wang, H. Which heads matter for reasoning? rl-guided kv cache compression. *arXiv preprint arXiv:2510.08525*, 2025.

Fabbri, A. R., Li, I., She, T., Li, S., and Radev, D. Multi-news: A large-scale multi-document summarization dataset and abstractive hierarchical model. In *Proceedings of the 57th annual meeting of the association for computational linguistics*, pp. 1074–1084, 2019.

Feng, Y., Lv, J., Cao, Y., Xie, X., and Zhou, S. K. Adakv: Optimizing kv cache eviction by adaptive budget allocation for efficient llm inference. *arXiv preprint arXiv:2407.11550*, 2024.

Fu, Y., Cai, Z., Asi, A., Xiong, W., Dong, Y., and Xiao, W. Not all heads matter: A head-level kv cache compression method with integrated retrieval and reasoning. *arXiv preprint arXiv:2410.19258*, 2024.

Gliwa, B., Mochol, I., Bieseck, M., and Wawer, A. Samsum corpus: A human-annotated dialogue dataset for abstractive summarization. *arXiv preprint arXiv:1911.12237*, 2019.

Guo, D., Xu, C., Duan, N., Yin, J., and McAuley, J. Longcoder: A long-range pre-trained language model for code completion. In *International Conference on Machine Learning*, pp. 12098–12107. PMLR, 2023.

Guo, Z., Kamigaito, H., and Watanabe, T. Attention score is not all you need for token importance indicator in kv cache reduction: Value also matters. *arXiv preprint arXiv:2406.12335*, 2024.

Huang, L., Cao, S., Parulian, N., Ji, H., and Wang, L. Efficient attentions for long document summarization. *arXiv preprint arXiv:2104.02112*, 2021.

Kočiský, T., Schwarz, J., Blunsom, P., Dyer, C., Hermann, K. M., Melis, G., and Grefenstette, E. The narrativeqa reading comprehension challenge. *Transactions of the Association for Computational Linguistics*, 6:317–328, 2018.

Li, X. and Roth, D. Learning question classifiers. In *COLING 2002: The 19th International Conference on Computational Linguistics*, 2002.

Li, Y., Huang, Y., Yang, B., Venkitesh, B., Locatelli, A., Ye, H., Cai, T., Lewis, P., and Chen, D. Snapkv: Llm knows what you are looking for before generation. *Advances in Neural Information Processing Systems*, 37:22947–22970, 2024.

Liu, A., Feng, B., Xue, B., Wang, B., Wu, B., Lu, C., Zhao, C., Deng, C., Zhang, C., Ruan, C., et al. Deepseek-v3 technical report. *arXiv preprint arXiv:2412.19437*, 2024.

Liu, T., Xu, C., and McAuley, J. Repobench: Benchmarking repository-level code auto-completion systems. *arXiv preprint arXiv:2306.03091*, 2023a.

Liu, Z., Wang, J., Dao, T., Zhou, T., Yuan, B., Song, Z., Shrivastava, A., Zhang, C., Tian, Y., Re, C., et al. Deja vu: Contextual sparsity for efficient llms at inference time. In *International Conference on Machine Learning*, pp. 22137–22176. PMLR, 2023b.

Lv, B., Zhou, Q., Ding, X., Wang, Y., and Ma, Z. Kypruner: Structural pruning for faster and memory-efficient large language models. In *ICASSP 2025-2025 IEEE International Conference on Acoustics, Speech and Signal Processing (ICASSP)*, pp. 1–5. IEEE, 2025.

Pope, R., Douglas, S., Chowdhery, A., Devlin, J., Bradbury, J., Heek, J., Xiao, K., Agrawal, S., and Dean, J. Efficiently scaling transformer inference. *Proceedings of machine learning and systems*, 5:606–624, 2023.

Roy, A., Saffar, M., Vaswani, A., and Grangier, D. Efficient content-based sparse attention with routing transformers. *Transactions of the Association for Computational Linguistics*, 9:53–68, 2021.

Tang, C., Liu, J., Xu, H., and Huang, L. Adaptive kv-cache compression without manually setting budget. *arXiv preprint arXiv:2509.03136*, 2025.

Tang, J., Zhao, Y., Zhu, K., Xiao, G., Kasikci, B., and Han, S. Quest: Query-aware sparsity for efficient long-context llm inference. *arXiv preprint arXiv:2406.10774*, 2024.

Vaswani, A., Shazeer, N., Parmar, N., Uszkoreit, J., Jones, L., Gomez, A. N., Kaiser, Ł., and Polosukhin, I. Attention is all you need. *Advances in neural information processing systems*, 30, 2017.

Voita, E., Talbot, D., Moiseev, F., Sennrich, R., and Titov, I. Analyzing multi-head self-attention: Specialized heads do the heavy lifting, the rest can be pruned. *arXiv preprint arXiv:1905.09418*, 2019.

Xiao, G., Tian, Y., Chen, B., Han, S., and Lewis, M. Efficient streaming language models with attention sinks. *arXiv preprint arXiv:2309.17453*, 2023.

Xiao, G., Tang, J., Zuo, J., Guo, J., Yang, S., Tang, H., Fu, Y., and Han, S. Duoattention: Efficient long-context llm inference with retrieval and streaming heads. *arXiv preprint arXiv:2410.10819*, 2024.

Yang, Z., Qi, P., Zhang, S., Bengio, Y., Cohen, W., Salakhutdinov, R., and Manning, C. D. Hotpotqa: A dataset for diverse, explainable multi-hop question answering. In *Proceedings of the 2018 conference on empirical methods in natural language processing*, pp. 2369–2380, 2018.

Zhang, Z., Sheng, Y., Zhou, T., Chen, T., Zheng, L., Cai, R., Song, Z., Tian, Y., Ré, C., Barrett, C., et al. H2o: Heavy-hitter oracle for efficient generative inference of large language models. *Advances in Neural Information Processing Systems*, 36:34661–34710, 2023.

Zhong, M., Liu, X., Zhang, C., Lei, Y., Gao, Y., Hu, Y., Chen, K., and Zhang, M. Zigzagkv: Dynamic kv cache compression for long-context modeling based on layer uncertainty. In *Proceedings of the 31st International Conference on Computational Linguistics*, pp. 8897–8907, 2025.

Zhou, X., Wang, W., Zeng, M., Guo, J., Liu, X., Shen, L., Zhang, M., and Ding, L. Dynamickyv: Task-aware adaptive kv cache compression for long context llms. *arXiv preprint arXiv:2412.14838*, 2024.

A. Proof of Theorem 4.1

Proof. Let $A^{(l,h)} \in \mathbb{R}^{T \times T}$ be the full attention matrix for head h in layer l . For a specific query at position t , the attention distribution over keys is given by the row vector $A_{t,:}^{(l,h)}$. The compressed attention matrix $\tilde{A}^{(l,h)}$ is constructed by retaining only the indices in the set $\mathcal{S}^{(l)}$, where $|\mathcal{S}^{(l)}| = B_l$. The resulting sparse distribution is re-normalized. A standard result in sparse attention analysis (Zhang et al., 2023) states that the L_1 distance between the full and compressed distributions is bounded by twice the probability mass of the discarded tokens:

$$\left\| A_{t,:}^{(l,h)} - \tilde{A}_{t,:}^{(l,h)} \right\|_1 \leq 2 \sum_{j \notin \mathcal{S}^{(l)}} A_{t,j}^{(l,h)}. \quad (\text{A1})$$

This inequality implies that the approximation error is strictly determined by the total attention weight of the evicted tokens.

In CompilerKV, the selection set $\mathcal{S}^{(l)}$ is determined by the stabilized utility score $\hat{u}_j^{(l)}$, defined as Eq. (10). The selection rule $\mathcal{S}^{(l)} = \text{Top-}B_l(\hat{u}^{(l)})$ ensures that we retain tokens with the highest weighted utility. Ideally, maximizing utility \hat{u} minimizes the discarded attention mass. However, the true attention $A_{t,j}^{(l,h)}$ for a specific head h may deviate from the aggregated utility.

We bound this deviation using the head reliability weight. The selection rule keeps tokens with high $\hat{u}_t^{(l)} = \max_k(u_t^{(l,k)}) / W_{\text{head}}[l, k]$. Since dividing by $W_{\text{min}}^{(l)}$ provides a conservative scaling factor. Specifically, the error contribution of pruned tokens is strictly controlled by their utility. Combining these, we obtain the bound in terms of the utility sum:

$$\sum_{j \notin \mathcal{S}^{(l)}} A_{t,j}^{(l,h)} = \frac{1}{W_{\text{head}}[l, h]} \sum_{j \notin \mathcal{S}^{(l)}} (W_{\text{head}}[l, h] \cdot A_{t,j}^{(l,h)}) \leq \frac{1}{W_{\text{min}}^{(l)}} \sum_{j \notin \mathcal{S}^{(l)}} u_j^{(l,h)}. \quad (\text{A2})$$

Substituting this back into inequality (A1) yields the first result:

$$\left\| A_{t,:}^{(l,h)} - \tilde{A}_{t,:}^{(l,h)} \right\|_1 \leq \frac{2}{W_{\text{min}}^{(l)}} \sum_{j \notin \mathcal{S}^{(l)}} u_j^{(l,h)}. \quad (\text{A3})$$

We now derive the bound for the Frobenius norm over the entire layer. The squared Frobenius norm of the error matrix $E^{(h)}$ for head h is:

$$\|E^{(h)}\|_F^2 = \sum_{t=1}^T \|A_{t,:}^{(l,h)} - \tilde{A}_{t,:}^{(l,h)}\|_2^2. \quad (\text{A4})$$

Using the norm inequality $\|x\|_2 \leq \|x\|_1$, we have $\|A_{t,:} - \tilde{A}_{t,:}\|_2^2 \leq \|A_{t,:} - \tilde{A}_{t,:}\|_1^2$. However, since probabilities sum to 1, a tighter bound for the specific case of probability distributions is $\|A_{t,:} - \tilde{A}_{t,:}\|_2 \leq \sqrt{2 \sum_{j \notin \mathcal{S}} A_{t,j}}$. Thus,

$$\|E^{(h)}\|_F \approx \sqrt{\sum_{t=1}^T \left(\sum_{j \notin \mathcal{S}} A_{t,j}^{(l,h)} \right)^2} \quad (\text{A5})$$

We define the random variable $X_t = \sum_{j \notin \mathcal{S}} A_{t,j}^{(l,h)}$ representing the ‘lost mass’ at step t . The expected value of the total lost mass is $\mathbb{E}[\sum X_t] = T \cdot \epsilon_{\text{tail}}^{(l)}$. By the McDiarmid’s Inequality (or Hoeffding’s bound for bounded variables), the deviation of the sum of independent random variables (assuming approximate independence of attention distributions across diverse prompts) from its expectation is bounded. The range of the sum is constrained by the number of pruned tokens ($T - B_l$). The sensitivity of the selection function is scaled by the inverse of the head reliability weights (since a low weight increases the variance of the selection decision).

Applying the concentration bound with probability $1 - \delta$:

$$\frac{1}{T} \sum_{t=1}^T X_t \leq \mathbb{E}[X_t] + \mathcal{O} \left(\sqrt{\frac{\log(1/\delta)}{T}} \right) \quad (\text{A6})$$

Scaling to the Frobenius norm (which involves \sqrt{T}):

$$\|E^{(h)}\|_F \leq \sqrt{T} \cdot \epsilon_{\text{tail}}^{(l)} + \mathcal{O}\left(\sqrt{\frac{(T - B_l) \log(1/\delta)}{T}}\right) \quad (\text{A7})$$

Finally, incorporating the $W_{\min}^{(l)}$ term to account for the worst-case head reliability (since we average over H heads, the bound is dominated by the least reliable head if not weighted), we arrive at the final aggregated bound:

$$\frac{1}{H} \sum_{h=1}^H \left\| A^{(l,h)} - \tilde{A}^{(l,h)} \right\|_F \leq \sqrt{T} \cdot \epsilon_{\text{tail}}^{(l)} + \mathcal{O}\left(\sqrt{\frac{(T - B_l) \log(1/\delta)}{T \cdot (W_{\min}^{(l)})^2}}\right) \quad (\text{A8})$$

This confirms that the approximation error is bounded by the tail mass ϵ_{tail} , and the stability of this bound improves as the context length T increases (law of large numbers), but is penalized by aggressive pruning ($T - B_l$) and low head reliability (W_{\min}). \square

B. Additional Experiments

B.1. Offline Table Compilation

Calibration corpus. We compile both decision tables (the head heterogeneity table $W_{\text{head}}[l, h]$ and the risk-adaptive threshold gating T_{gate}) on a held-out *calibration corpus* \mathcal{D}_{cal} , which is strictly disjoint from the LongBench evaluation set to avoid leakage. \mathcal{D}_{cal} contains approximately 50K long-context prompts sampled from diverse public sources, including long-form narratives (PG19), scientific/technical articles (arXiv, PubMed), long-document summarization and meeting transcripts (GovReport, QMSum, BookSum), as well as instruction-style dialogues and code/QA text (ShareGPT/UltraChat and The Pile subsets such as GitHub/StackExchange). All prompts are used in an unlabeled manner: we only require forward statistics from the prefill stage and a short continuation loss for reward computation.

Risk signals and stratified coverage. For each prompt $x_{1:T}$, we compute the observation-window statistics on $\mathcal{W} = \{T - w_{\text{obs}} + 1, \dots, T\}$, including the attention entropy $H(A)$ and local perplexity, and discretize them into bin indices (b_h, b_p) . To ensure sufficient coverage of high-risk prompts (e.g., high-entropy or high-perplexity regimes), we adopt stratified sampling over (b_h, b_p) when constructing \mathcal{D}_{cal} , avoiding a dominance of medium-risk samples that would otherwise bias the learned tables toward overly aggressive pruning.

Why 20×4 bins for $(H(A), \text{PPL})$. We choose $N_H=20$ entropy bins and $N_P=4$ perplexity bins, resulting in a 20×4 risk grid for each layer. This design is motivated by a practical bias-variance trade-off for discrete table policies: (i) attention entropy is a *structural* signal with a relatively smooth and wide dynamic range over long-context prompts, hence we allocate finer granularity (20 bins) to capture gradual shifts in concentration vs. dispersion; (ii) perplexity acts as a *semantic uncertainty* signal whose main role is to modulate the overall conservativeness, and empirically exhibits heavier tails and higher estimation noise on short windows, thus we use coarser partitioning (4 bins) to maintain stability. With $L=32$ layers, the LUT contains $32 \times 20 \times 4 = 2560$ entries, which is small enough for robust offline estimation and deployment, while still expressive enough to differentiate risk regimes without introducing over-fragmentation. In our calibration, this binning yields adequate per-cell support under stratified sampling and avoids sparse high-risk cells that would cause unstable threshold decisions.

Model choice and cross-architecture applicability. We compile tables on a 32-layer backbone to obtain a unified layer index space. For models with different depths, we apply a monotonic depth mapping (e.g., relative-depth interpolation) at inference time. While our main results use per-model compilation, we also explore depth mapping as a heuristic to reuse tables across similar 7B–8B backbones, with preliminary evidence suggesting potential portability. We leave a rigorous same-table transfer evaluation for future work.

Hyperparameter ranges and robustness. Both compiled tables operate as *bounded multiplicative modulators* on top of a normalized utility signal, which allows us to use conservative and architecture-stable ranges. For Stage 3, the LUT outputs a layer threshold $\tau^{(l)} \in [0.8, 1.0]$. This range is chosen for two reasons. First, $\hat{u}_t^{(l)}$ is constructed from the stabilized utility $u_t = \alpha_t \cdot \rho_t$, where ρ_t is sample-normalized; empirically, this makes $\hat{u}_t^{(l)}$ concentrate around $\mathcal{O}(1)$ across prompts

Table A1. Efficiency comparison between FullKV and our CompilerKV. CompilerKV compiles a fixed compressed KV-cache before decoding, enabling faster token generation with slightly higher prefill cost (TTFT) but significantly improved end-to-end latency and memory usage.

Context Setting			Efficiency Metrics			
Input (Tok)	Output (Tok)	Method	TTFT (s) \downarrow	TPOT (tok/s) \uparrow	Latency (s) \downarrow	Memory (MB) \downarrow
8k	2k	FullKV	0.66	27.63	74.79	20055
		CompilerKV	0.72	36.20	58.90	19050
16k	4k	FullKV	1.45	19.55	209.56	23859
		CompilerKV	1.52	34.80	118.40	21420
32k	8k	FullKV	3.52	11.65	706.56	31213
		CompilerKV	3.65	28.50	285.00	26880

and layers, so thresholds outside $[0.8, 1.0]$ either admit almost all tokens (too conservative) or reject nearly all tokens (degenerate), collapsing the “threshold+Top- B_l ” mechanism. Second, under tight budgets the final retention is always enforced by Top- B_l ; hence $\tau^{(l)}$ mainly controls the *candidate set margin* rather than the final budget. Bounding $\tau^{(l)}$ to $[0.8, 1.0]$ keeps the candidate size within a stable, budget-aligned regime while still allowing risk-conditioned shifts across (b_h, b_p) .

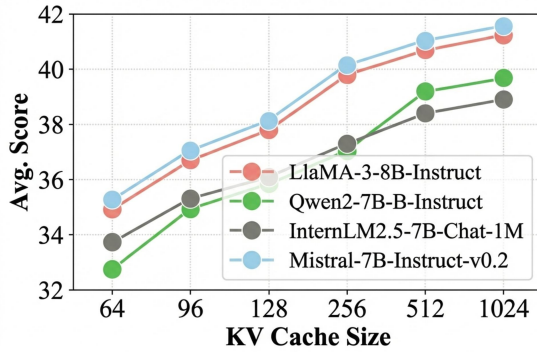


Figure A1. Universality across Model Architectures. The average performance trend of our method on four different LLMs (LLaMA-3, Qwen2, InternLM-2.5, Mistral) under varying KV cache budgets (ranging from 64 to 1024). The consistent degradation patterns across diverse architectures demonstrate the generalization capability of our risk-adaptive mechanism.

B.2. Runtime Efficiency and Memory Analysis

To evaluate the practical deployment viability of CompilerKV, we conducted a comprehensive efficiency profile comparing it against the lossless FullKV baseline. We measured Time to First Token (TTFT), Time Per Output Token (TPOT), end-to-end Latency, and Peak Memory usage across varying context lengths (Input: 8k-32k, Output: 2k-8k). The results are detailed in Table A1.

Prefill Overhead vs. Decoding Speedup. As shown in the “TTFT” column, CompilerKV introduces a marginal overhead during the prefill phase (e.g., an increase from 0.66s to 0.72s in the 8k setting). This slight delay is the expected “compilation cost” incurred by our Risk-Adaptive Gating and Head-Aware Importance calculation. However, this one-time investment yields significant returns during the decoding phase. By strictly maintaining a compressed budget, CompilerKV dramatically improves the throughput (TPOT). For instance, in the 32k input scenario, the generation speed increases from 11.65 tok/s to 28.50 tok/s.

End-to-End Latency. Consequently, the total latency sees a substantial reduction. The slight delay in prefill is negligible compared to the time saved during generation. In the most demanding setting (32k input, 8k output), CompilerKV reduces

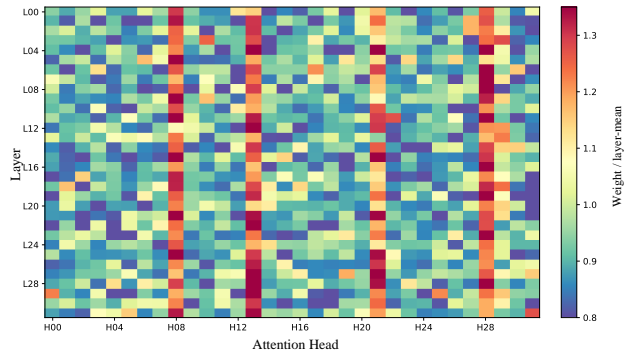


Figure A2. Visualization of Learned Head Reliability Table. The color intensity represents the learned scaling factor for each head across layers. The emergence of distinct suppressed zones (blue/cold colors) confirms that our method automatically identifies and suppresses noisy heads that would otherwise disrupt token selection.

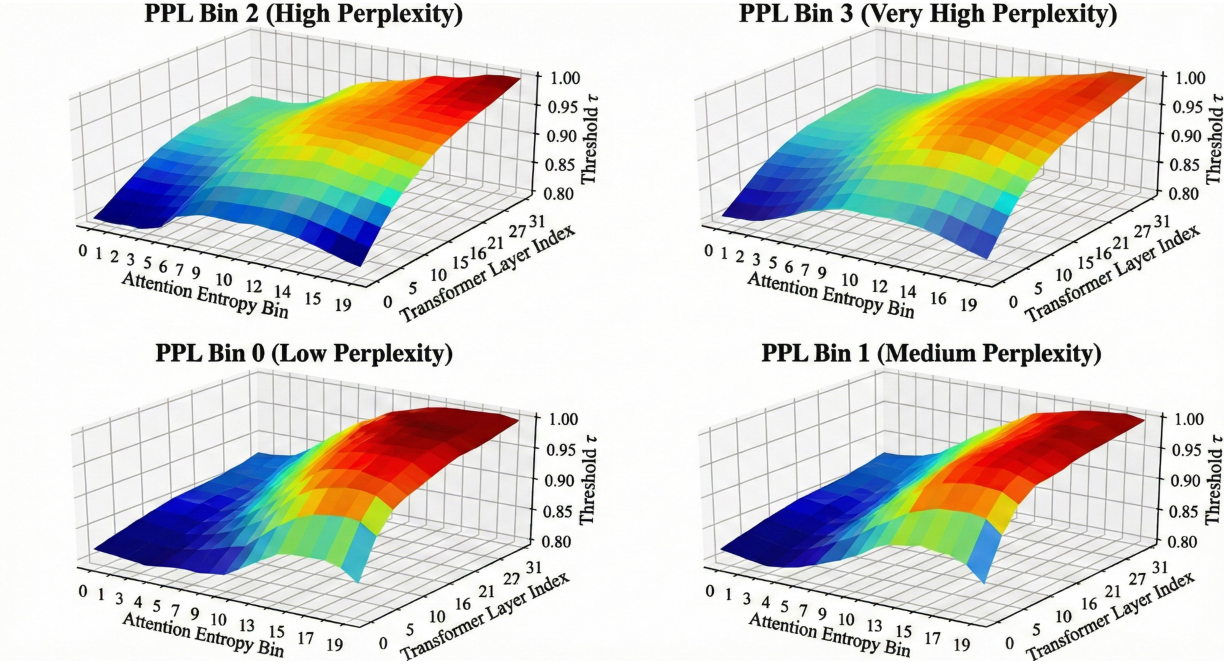


Figure A3. Risk-Adaptive Threshold Gating Policy. The plots show the learned retention threshold (τ) across layers for samples with varying risk levels (binned by Perplexity and Attention Entropy). For high-risk samples (High Perplexity, rightmost plots), the policy automatically lowers thresholds to preserve more information, validating our risk-adaptive mechanism.

the total latency by approximately 60% (from 706.56s to 285.00s), demonstrating that the "compile-then-execute" paradigm is highly efficient for long-context generation tasks.

Memory Efficiency. Furthermore, CompilerKV consistently reduces peak memory consumption. By proactively filtering redundant historical states, it saves approximately 14%–16% of GPU memory compared to FullKV, alleviating hardware bottlenecks and enabling longer context processing on resource-constrained devices.

Universality across Model Architectures. Figure A1 demonstrates our method's consistent performance trajectory across four distinct LLMs (including LLaMA-3, Qwen2, and Mistral) as the budget tightens from 1024 to 64 tokens. This architectural universality confirms that our Risk-Adaptive Gating and Head Reliability mechanisms capture fundamental attention properties rather than overfitting to specific model weights.

B.3. Visualization of Learned Policies

To understand how CompilerKV adapts to different risk levels, we visualize the learned threshold table \mathbf{T}_{gate} in Figure A3. The visualization confirms that the offline RL process converges to an interpretable strategy: As shown in the difference between the "Low Perplexity" and "High Perplexity" subplots, the policy globally lowers the retention threshold (blue zones) for high-perplexity samples, allowing more tokens to be stored when the model is uncertain. Within each plot, as Attention Entropy increases (x -axis), the threshold decreases. This indicates the model automatically acts conservatively for diffuse attention patterns (e.g., dense retrieval), preventing the pruning of scattered but critical information.

We visualize our learned Head Reliability Table in Figure A2. The heatmap reveals a clear structure: specific heads (e.g., in middle layers L12–L20) are consistently assigned negative or low weights, indicating they act as "noise emitters" for the prefill task. By explicitly down-weighting these heads, our Pass-3 mechanism prevents them from polluting the budget with irrelevant tokens.

C. Algorithm

Model	Method	Single-Document QA				Multi-Document QA				Summarization				Few-shot Learning				Synthetic			Code												
		NrvQA		Qasper		MF-en		HotpotQA		2WikiMQA		Musique		GovReport		QMSum		MultiNews		TRFC		TriviaQA		SAMSum		PCount		PRe		Lcc		RB-P	
		18409	3619	4559	9151	4887	11214	8734	10614	2113	5177	8209	6258	11141	9289	1235	4206	–	–	–	–	–	–	–	–	–	–	–	–	–			
LLaMA-3.8B -Instruct	FullKV	25.16	31.81	39.59	43.09	36.15	21.77	28.62	23.34	26.33	75.00	90.50	42.36	5.20	69.25	59.04	53.93	41.95	–	–	–	–	–	–	–	–	–	–	–	–			
	StreamingLLM	17.85	9.50	23.09	37.84	29.02	16.77	17.91	20.42	20.16	44.00	73.00	30.00	5.80	69.50	48.38	49.31	32.03	–	–	–	–	–	–	–	–	–	–	–	–			
	H2O	21.58	12.54	28.49	37.13	32.36	18.88	20.23	22.16	21.14	39.00	86.62	39.19	5.50	69.50	57.39	54.46	35.39	–	–	–	–	–	–	–	–	–	–	–	–			
	SnapKV	21.71	12.37	32.38	37.44	30.48	19.50	19.06	21.36	20.07	45.5	87.74	38.15	5.50	68.85	57.42	54.61	35.76	–	–	–	–	–	–	–	–	–	–	–	–			
	PyramidKV	22.26	16.65	30.73	38.97	29.28	19.19	19.92	22.06	20.87	68.00	88.95	38.23	5.92	69.50	57.20	51.54	37.45	–	–	–	–	–	–	–	–	–	–	–	–			
	DynamicKV	22.10	14.93	32.94	41.06	27.98	21.18	20.03	22.06	21.28	65.50	89.61	38.70	5.13	69.50	58.01	54.00	37.75	–	–	–	–	–	–	–	–	–	–	–	–			
Mistral-7B -Instruct-v0.2	FullKV	26.63	32.99	49.34	42.77	27.35	18.77	32.87	24.24	27.10	71.00	86.23	42.96	2.75	86.98	56.93	54.49	42.71	–	–	–	–	–	–	–	–	–	–	–	–			
	StreamingLLM	16.58	14.76	30.36	28.13	21.76	11.98	18.26	19.02	19.16	43.50	74.12	28.50	2.50	31.81	43.65	41.19	27.83	–	–	–	–	–	–	–	–	–	–	–	–			
	H2O	21.66	21.64	38.60	30.96	20.63	13.02	20.65	22.61	22.08	39.00	82.19	39.75	3.16	79.98	51.25	48.20	34.71	–	–	–	–	–	–	–	–	–	–	–	–			
	SnapKV	20.11	21.28	42.98	37.51	22.31	14.43	19.19	21.89	21.01	48.00	83.77	40.44	2.51	66.99	51.64	48.57	35.16	–	–	–	–	–	–	–	–	–	–	–	–			
	PyramidKV	22.11	22.52	43.04	33.57	22.98	15.69	20.56	22.52	21.36	65.50	83.84	40.03	2.89	67.26	51.51	46.42	36.36	–	–	–	–	–	–	–	–	–	–	–	–			
	DynamicKV	22.05	23.65	43.08	36.03	22.60	15.23	21.35	23.11	22.19	68.00	84.79	41.02	4.20	70.11	52.45	47.41	37.33	–	–	–	–	–	–	–	–	–	–	–	–			
Qwen2-7B -Instruct	FullKV	25.14	42.35	45.04	14.80	14.13	9.23	36.35	23.79	26.51	76.50	89.16	45.23	6.50	75.50	60.30	60.78	40.71	–	–	–	–	–	–	–	–	–	–	–	–			
	StreamingLLM	19.25	23.63	26.51	14.00	15.30	7.46	18.07	19.30	18.30	47.00	77.92	31.57	6.50	17.00	42.52	41.94	26.64	–	–	–	–	–	–	–	–	–	–	–	–			
	H2O	20.33	30.43	34.22	13.61	13.37	7.81	20.72	21.66	18.44	40.00	86.94	42.17	7.00	70.50	53.45	53.76	33.40	–	–	–	–	–	–	–	–	–	–	–	–			
	SnapKV	22.26	31.62	38.95	16.05	17.71	7.66	18.91	21.41	18.21	46.00	87.61	42.01	6.50	63.50	54.87	53.03	34.14	–	–	–	–	–	–	–	–	–	–	–	–			
	PyramidKV	20.50	31.70	39.95	18.54	18.54	8.85	19.24	20.47	18.18	60.00	87.98	39.71	7.00	49.00	48.77	47.91	33.52	–	–	–	–	–	–	–	–	–	–	–	–			
	DynamicKV	22.77	35.57	42.62	14.80	16.35	8.31	21.41	21.97	19.56	58.00	88.18	40.93	6.50	70.00	53.58	52.50	35.82	–	–	–	–	–	–	–	–	–	–	–	–			
InternLM-2.5-7B -Chat-1M	FullKV	23.12	35.93	42.81	14.85	16.45	8.40	21.62	22.47	19.74	60.00	88.38	41.05	6.50	70.50	53.44	52.79	36.13	–	–	–	–	–	–	–	–	–	–	–	–			
	StreamingLLM	17.91	13.02	24.31	24.27	16.01	11.29	17.29	20.62	18.06	48.5	67.53	21.93	0.82	87.39	43.45	42.79	29.70	–	–	–	–	–	–	–	–	–	–	–	–			
	H2O	16.16	17.71	27.94	26.83	17.83	17.81	13.99	22.59	16.9	39.50	81.87	32.15	1.32	96.50	48.30	47.27	32.79	–	–	–	–	–	–	–	–	–	–	–	–			
	SnapKV	19.65	17.44	35.29	27.36	18.58	19.79	12.76	22.42	16.31	48.00	80.23	31.35	0.95	95.00	49.47	48.22	33.93	–	–	–	–	–	–	–	–	–	–	–	–			
	PyramidKV	18.80	17.35	33.48	31.16	20.05	19.02	14.65	22.02	17.40	69.50	80.87	32.02	1.23	95.00	47.13	44.73	35.28	–	–	–	–	–	–	–	–	–	–	–	–			
	DynamicKV	17.93	19.89	34.15	31.50	19.03	20.60	15.14	22.41	18.15	70.00	83.09	32.44	0.86	95.50	49.33	47.16	36.07	–	–	–	–	–	–	–	–	–	–	–	–			
InternLM-2.5-7B -Chat-1M	CompilerKV	18.36	20.32	34.61	32.17	19.75	20.95	15.5	22.62	18.46	70.50	83.43	32.76	0.92	97.00	49.28	47.42	36.50	–	–	–	–	–	–	–	–	–	–	–	–			

Table A2. Performance comparison on the LongBench dataset for full KV cache, previous methods (StreamingLLM, H2O, SnapKV, PyramidKV, DynamicKV), and our CompilerKV method, with KV cache sizes of 128, using models including LLaMA3-8B-Instruct, Mistral-7B-Instruct-v0.2, QWen2-7B-Instruct, and InternLM-2.5-Chat-1M. Bold indicates the best performance.

Algorithm 1 COMPILERKV: Prefill-only KV Compression (operator form)

1: **Input:** prompt $x_{1:T}$; layers $l \in [1, L]$; heads $h \in [1, H]$; per-layer budgets $\{B_l\}$; observation window $\Omega = \{T - w_{\text{obs}} + 1, \dots, T\}$; risk LUT \mathbf{T}_{gate} ; head table \mathbf{W}_{head}

2: **Output:** compressed KV cache $\{(\tilde{K}^{(l)}, \tilde{V}^{(l)})\}_{l=1}^L$

3: **(A) Prefill-time risk coordinates (streaming reductions)**

4: $\{A^{(l,h)}, K^{(l,h)}, V^{(l,h)}\} \leftarrow \text{PREFILL}(x_{1:T})$

5: $\bar{A} \leftarrow \text{MEAN}_{l,h}(A^{(l,h)})$

6: $\alpha \leftarrow \sum_{j \in \Omega} \bar{A}_{j,:} \in \mathbb{R}^T$

7: $\bar{A}' \leftarrow \alpha / \|\alpha\|_1$

8: $\mathcal{R}_{\text{struct}} \leftarrow \mathsf{H}(\bar{A}') = -\sum_{t=1}^T \bar{A}'_t \log \bar{A}'_t$

9: $\mathcal{R}_{\text{sem}} \leftarrow \exp\left(-\frac{1}{|\Omega|} \sum_{j \in \Omega} \log P(x_j | x_{<j})\right)$

10: $(b_{\text{ent}}, b_{\text{ppl}}) \leftarrow \text{DISCRETIZE}(\mathcal{R}_{\text{struct}}, \mathcal{R}_{\text{sem}})$

11: **(B) Stage 1: Stabilized token utility (vectorized)**

12: **for** $l = 1$ **to** L **do**

13: **for** $h = 1$ **to** H **do**

14: $r^{(l,h)} \leftarrow \|V^{(l,h)}\|_{2,\text{row}} \in \mathbb{R}^T$

15: $\mu^{(l,h)} \leftarrow \text{MEAN}_t(r^{(l,h)})$

16: $\rho^{(l,h)} \leftarrow r^{(l,h)} / (\mu^{(l,h)} + \epsilon) \in \mathbb{R}^T$

17: $u^{(l,h)} \leftarrow \alpha \odot \rho^{(l,h)} \in \mathbb{R}^T$

18: **end for**

19: **end for**

20: **(C) Stage 2: Head-aware importance injection (weighted max-pool)**

21: **for** $l = 1$ **to** L **do**

22: $\hat{u}^{(l)} \leftarrow \text{MAXPOOL}_h(u^{(l,h)} \odot \mathbf{W}_{\text{head}}[l, h]) \in \mathbb{R}^T$

23: **end for**

24: **(D) Stage 3: Risk-adaptive gating + budget correction**

25: **for** $l = 1$ **to** L **do**

26: $\tau^{(l)} \leftarrow \mathbf{T}_{\text{gate}}[l, b_{\text{ent}}, b_{\text{ppl}}]$

27: $m^{(l)} \leftarrow \mathbb{I}[\hat{u}^{(l)} \geq \tau^{(l)}] \in \{0, 1\}^T$

28: $\mathcal{S}^{(l)} \leftarrow \text{SELECT}(\hat{u}^{(l)}, m^{(l)}, B_l)$

29: $(\tilde{K}^{(l)}, \tilde{V}^{(l)}) \leftarrow \text{GATHER}_{\text{tok}}(K^{(l)}, V^{(l)}; \mathcal{S}^{(l)})$

30: **end for**

31: **return** $\{(\tilde{K}^{(l)}, \tilde{V}^{(l)})\}_{l=1}^L$

32: // **SELECT:** if $\|m^{(l)}\|_0 \leq B_l$, keep all candidates; else return Top- B_l indices under score $\hat{u}^{(l)}$.

33: // **GATHER_{tok}** gathers along token dimension; $\mathcal{S}^{(l)}$ is shared across heads within layer l .
